

Original Research Paper

# CuInSe<sub>2</sub> (CIS) as A light Absorption Layer of Photovoltaic Solar-Cells

Omar Abdulsada Ali

Department of Physics, College of Science, University of Baghdad, Baghdad, Iraq

## Article history

Received: 22-06-2015

Revised: 18-02-2016

Accepted: 29-02-2016

## Corresponding Author:

Omar Abdulsada Ali  
Department of Physics, College  
of Science, University of  
Baghdad, Baghdad, Iraq  
E-mail: omarlibra2005@yahoo.com

**Abstract:** Arrested precipitation method used to synthesize CuInSe<sub>2</sub> (CIS) nanocrystals were added to a hot solvent with organic capping ligands to control nanocrystal formation and growth. CIS thin films deposited onto Soda-Lime Glass (SLG) substrate by spray-coat, then selenized in Ar-atmosphere to form CIS thin films. PVs were made with power conversion efficiencies of 0.631% as-deposited and 0.846% after selenization, for Mo coated, under AM 1.5 illuminations. (XRD) and (EDX) it is evident that CIS have chalcopyrite structure as the major phase with a preferred orientation along (112) direction and Cu:In:Se nanocrystals is nearly 1:1:2 atomic ratio.

**Keywords:** CuInSe<sub>2</sub>, Nanoink, Arrested Precipitation, Selenization, Ar-Atmosphere, Photovoltaic, Chalcopyrite

## Introduction

CIS and (CIGS) chalcopyrite semiconductors are considered popular as a light absorption layer of Photovoltaics (PV<sub>s</sub>). In the past and now used PV<sub>s</sub> materials, like silicon, is not perfect due to its high production cost and low efficiency ( $\mu$ ). Therefore, chalcopyrite semiconductor such as CIS, which has low cost and high ( $\mu$ ), is predicted in the next generation to be Photovoltaic Solar Cells (PVSC<sub>s</sub>) materials. CIS can be synthesized as thin film. Moreover, has a large light absorption coefficient and appropriate direct band gap is good for the absorption of sunlight. self-regeneration function of CIS is relatively easy to process it (Zhang *et al.*, 1998; Tani *et al.*, 2012). CIS now is one of the most promising materials for photovoltaic solar cell applications. CIS alloys have suitable band gaps, suitable work functions, mobilities to serve as PV absorber layers, suitable charge densities and high optical absorption coefficients. Today CIS achieved efficiency of 18.8% as a copper based solar cell (Bindu *et al.*, 2003). Band gap of CIS is (1.04 eV) and has a good absorption coefficient ( $10^5 \text{ cm}^{-1}$ ) for solar spectrum make this material an excellent candidate for a solar cell absorber layer (Ider *et al.*, 2014; Tesson *et al.*, 1998). Many methods are used for the synthesis of CIS films like elemental co-evaporation (Szot and Haneman, 1984), sputtering (Parretta *et al.*, 1993) and electro deposition (Tzvetkova *et al.*, 1997). These methods become necessary to produce device quality CIS films through a low-cost, eco-friendly and easily

scalable process for mass production of films for PV applications. Co-evaporation of the elements (Szot and Haneman, 1984) and annealing of Cu-In precursors in H<sub>2</sub>Se/Se atmosphere (Verma *et al.*, 1996; Schmidt *et al.*, 1994) are the most widely accepted methods. Both processes are extremely toxic to health and environment due to use Se vapor or H<sub>2</sub>Se gas.

In this study, Arrested precipitation method used to synthesize CuInSe<sub>2</sub> (CIS) nanocrystals were added to a hot solvent with organic capping ligands to control nanocrystal formation and growth. Arrested precipitation has been a particularly effective way to obtain nanocrystals with a wide range of compositions and tunable sizes and shapes (Akhavan *et al.*, 2012; Stolle *et al.*, 2013). Mo/CIS layers deposited onto SLG substrate by spray-coat and selenized in Ar-atmosphere to form CIS thin films.

## Experiments

Soda-Lime Glass (SLG) (25×25×1.1 mm Delta Technologies), Cr (99.999%, Lesker), Molybdenum (Mo) (Lesker 99.95%), ZnO target (Lesker, 99.9%) in a 0.5% O<sub>2</sub> in Ar atmosphere (Praxair, 99.95%) and ITO target (Lesker, 99.99% In<sub>2</sub>O<sub>3</sub>:SnO<sub>2</sub> 90:10) in Ar atmosphere (Praxair, research grade) oleylamine (OLA; >70%), Diphenylphosphine (DPP; 97%), copper(I) chloride (CuCl; 99.995+%), indium(III) chloride (InCl<sub>3</sub>; anhydrous 99.99%), elemental selenium (Se, 99.99%), cadmium sulfate (CdSO<sub>4</sub>, 99.999%) from Aldrich Chemical Co.; Ammonium hydroxide (18 M

NH<sub>4</sub>OH), toluene, ethanol, were obtained from Fisher Scientific; and thiourea (99.999%) from Fluka Co.; Oleylamine was degassed by pulling vacuum overnight at ~200 mTorr at 110°C and stored in an N<sub>2</sub> filled glovebox before use. All other chemicals were used as received without further purification. CuCl, InCl<sub>3</sub>, DPP and degassed OLA were stored in a N<sub>2</sub>-filled glovebox to prevent degradation.

CIS nanocrystals were prepared by procedures in (Akhavan *et al.*, 2010a; 2010b; Stolle *et al.*, 2012). In a typical reaction, (0.45 g) of copper(I) chloride, (1.11 g) of indium(III) chloride and 13 mL of degassed OLA are added to a 100 mL three-neck flask after cleaning which input inside an N<sub>2</sub> filled glovebox (name solution 1). Reaction 4 mmol of Se, 2 mL of degassed OLA and 1.5 mL of DPP added to vial of 25 mL (name solution 2) stirrer and heat into dissolve. The flask of sol. 1 is put in a Schlenk line and degassed under a vacuum at 110°C for 30 min. The flask is then filled with N<sub>2</sub> and heated to 240°C for 1 h and when the temperature reached to 180°C injected the sol. 2 was injected, the color of solution changed to black immediately. The reaction was cooling to the room temperature after the heating mantle is removed. The resulted nanocrystals are washed by centrifugation using toluene and ethanol. Mixed 10 mL of ethanol with contents of the reaction vessel in a glass centrifuge tube and the nanocrystal product is precipitated by centrifugation at 6000 rpm for 3 min, so supernatant is discarded. The product nanocrystals is redispersed in 5 mL of toluene and centrifuged at 6000 rpm for 3 min to remove the larger and poorly capped product. The supernatant is added to a new glass centrifuge tube and the precipitate is discarded. Ethanol is then slowly added to the nanocrystals dispersion until the mixture becomes slightly turbid. The mixture is centrifuged at 6000 rpm for 3 min to again precipitate the nanocrystal product. The supernatant is discarded and the solid product is redispersed in toluene to a final concentration of 20 mg mL<sup>-1</sup>. Then nanocrystals dispersion is transferred to a glovebox for the ligand exchange.

Selenization of nanocrystal films took place inside a graphite cylinder, sealed and purged with pure Ar to achieve an inert atmosphere. The tube furnace was heated up to selenization temperature typically 525°C for 60 min and then cooled down to the room temperature. The graphite cylinder was opened within an inert atmosphere glovebox and the films were removed and saved in the glovebox.

For morphological structure studies, Transmission Electron Microscopy (TEM) was performed using a JEOL 2010F TEM at 200 kV accelerating voltage. TEM samples were prepared by drop casting from chloroform onto a 200 mesh nickel grid with a carbon film (Electron Microscopy Sciences). Energy

Dispersive X-ray (EDX) was carried out using an Oxford INCA EDS detector on the JEOL 2010F TEM. Scanning Electron Microscopy (SEM) was performed on a Zeiss Supra 40 VP SEM operated at 5 keV accelerating voltage through an In-lens detector with samples grounded using copper tape.

For structural study X-Ray Diffraction (XRD) was performed using a Rigaku R-Axis Spider diffractometer with an image-plate detector and Cu K $\alpha$  ( $\lambda = 1.54 \text{ \AA}$ ) radiation operated at 40 kV and 40 mA. XRD samples were prepared by drying a drop of concentrated nanoparticle dispersion onto a glass slide in a glovebox. The nanocrystal powder was then suspended on a 0.5 mm nylon loop using mineral oil for analysis. Samples were scanned for 15 min while rotating at 2°/s. The 2D diffraction patterns were integrated using the Rigaku 2DP powder processing suite with subtraction of the background scattering from the nylon loop and mineral oil.

Conductive back contacts Mo were deposited separately on sodalime glass after cleaned by sonication in an isopropanol and acetone mixture, followed by rinse with (DI) water and drying under a N<sub>2</sub>. Molybdenum of 500 nm thick was deposited by RF sputtered while the Au was thermally evaporated. 10 mg mL<sup>-1</sup> solutions of nanoparticles were prepared for the spray-coating. CIS nanocrystal layers were spray-coated with an airbrush (SONOTEK) operated at 1.6 psig of head pressure. CdS was deposited as a buffer layer by (CBD) following procedures described by McCandless and Shafarman (2003). A buffer layer was deposited by dropping 0.7 mL of a CdS precursor solution (1.25 mL of 15 mM CdSO<sub>4</sub>, 2.2 mL of 1.5 M thiourea and 2.8 mL of 18 M NH<sub>4</sub>OH in water) onto the CIS nanocrystal film and heated to 95°C on a hot plate and covered with an inverted crystallization dish for 2 min. Removed The substrate from the hot plate, rinsed with distilled water and dried by compressed air. ZnO and ITO were deposited by RF sputtering from a 40 nm ZnO target and a 300 nm of ITO target. Top layers of ZnO/ITO are deposited onto rectangular regions with active device areas of (8 mm<sup>2</sup> a 4×2 mm rectangle). Silver paste was used for electrical contact of the devices.

PV device response was measured using a Keithley 2400 General Purpose Sourcemeter under solar simulation using a Newport Xenon Lamp Solar Simulator with an AM 1.5 filter (100 mW/cm<sup>2</sup>). Intensity of the light source was calibrated using a NIST calibrated Si photodiode (Hamamatsu, S1787-08). Different fractions of solar spectrum were generated by placing colored glass cutoff filters (Newport) directly in the path of light beam emanating from the solar simulator. Incident Photon Conversion Efficiency (IPCE) was measured using a home-built device with

lock-in amplifier (Stanford Research Systems, model SR830) and monochromator (Newport Cornerstone 260 1/4M). IPCE was calibrated with Si and Ge photodiodes (Hamamatsu).

## Results

Figure 1 shows Cu:In:Se atomic ratio in the nanocrystals measured by EDX is nearly 1:1:2.

The nanoink disperse in various organic solvents contains chloroform, toluene and acetone. Toluene was used as the dispersing solvent for the nanoinks which is used to fabricate devices, as it provided the most uniform coatings of the solvents that were tested. Table 1 summarizes the composition of CIS nanoink determined by EDS.

Figure 2 shows TEM images for the OLA capped CIS nanoinks. The nanocrystals are composed of chalcopyrite CIS. TEM images of CIS nanoinks shows the nanocrystals are irregularly shaped and rather polydisperse.

Figure 3A shows all the various peaks in the XRD pattern can be indexed to phase of CIS films deposited on SLG substrates annealed at 525°C with chalcopyrite tetragonal structure, which are in good agreement with the standard values of the reported data (JCPDS No.40-1487) as the major phase and no secondary phase with a preferred orientation along (112) direction. The two weak peaks including (211) and (400) at ( $2\theta = 35^\circ$  and  $64^\circ$ ) emerge here that recognize the chalcopyrite phase from the sphalerite phase. In addition, no peaks of other impurities were detected before annealing, indicating the high phase purity of CIS samples. From the figures one can observe that CIS films are polycrystalline structure where many peaks appeared.

An ideal feature is that, in all the range of compositions obtained, the samples exhibit a strong preference orientation, the most intense peak is situated at nearly  $26.50^\circ$  which is belong to Miller indices. As could be seen from the XRD patterns, the three main diffraction peaks due to (112), (220) and (312) planes which are belong to ( $2\theta = 26.58^\circ$ ,  $44.18^\circ$  and  $52.34^\circ$ ) correspond to CIS.

In contrast, low intensity (112), (220) and (312) peaks were observed in the film before selenization. The diffraction peaks intensity improves with long time selenization.

Figure 3B shows (112) CIS diffraction peak is broad for films without annealing and baking, the (112) peak due to the CIS ( $2\theta = 26.58^\circ$ ) become narrower after annealing at 525°C for 1 h in Ar atmosphere., which corresponds to the presence of large particles as will show in SEM images.

The morphology of the CIS synthesized at 240°C for 1 hour shown in Fig. 4. The product is mainly composed

of a large amount of nanoparticles after annealing and these CIS nanoparticles with irregular shapes were easily aggregated together.

It is clear from the figures that the film surface had relatively homogeneous polycrystalline grain structure. The surface morphology shows that the CIS composition before annealing (as deposition) has a small grain size and smooth surface but become nearly uniform and dense surface with visible boundary after annealing. When annealing CIS composition, the grain size become much larger than the grain size in as-deposition composition.

The heat treatment at 525°C for 4 h in Ar atmosphere is an important factor for producing bigger layer thickness which used for condense the homogeneity and improve the layer thickness of CIS thin film.

Small sintering observed for lower temperature deposition, but not for higher temperature. This could be related to the amount of solvent on the film during deposition. At higher temperatures, the film appears more uniform. Sintering occurs to a small extent, similar to the low temperature spray cast films.

The I-V response for the forward and reverse bias voltages of device architecture consisting of layers of glass/Mo/CIS/CdS/ZnO/ITO solar cell fabricated before and after selenization is shown in Fig. 5 for thicknesses of 150 nm and concentration  $10 \text{ mg mL}^{-1}$  of CIS DPP: Senanocrystal layer deposited by spray-coating before and after selenization. It is clear that (PCE) increased after selenization from 0.631 to 0.846%.

Also it can be seen from these figure that for all samples, the forward current increases selenization. These may be due to the increase of carrier concentration which affected the energy band bending and thus result in a decreasing in depletion region width. In the reverse bias, the depletion region increases due to introduction of high barrier potential (Cullity, 1967). Reverse current increases with increasing bias voltage. The saturated current at reverse bias can be explained on the basis of the lack of tunneling mechanism (Katagiri *et al.*, 2001).

One can notice that the illumination current increases with increasing of concentration  $x$  which is cause the increasing in the grain size and reducing of grain boundaries which lead to the increase of the mobility and increase the illumination current, the value of solar cell parameters.

Table 1. The Composition of CuInSe<sub>2</sub> nanoink determined by EDS

Nanoink	Element	Weight %	Atomic %
CIS DPP:Se	Cu K	21.46	27.88
	In L	30.60	22.00
	Se L	47.94	50.12

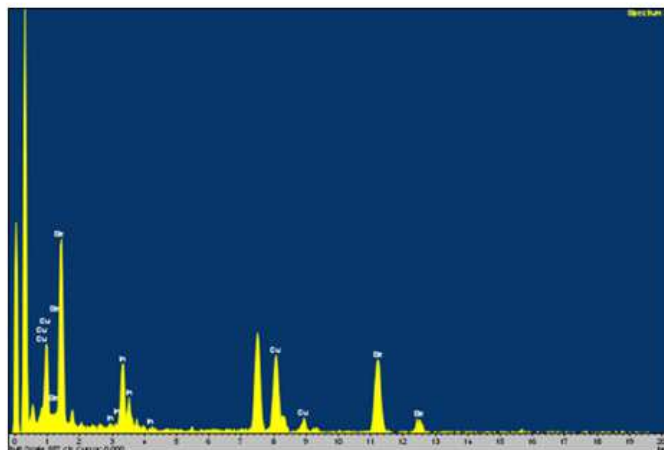


Fig. 1. EDS pattern of CIS DPP:Se

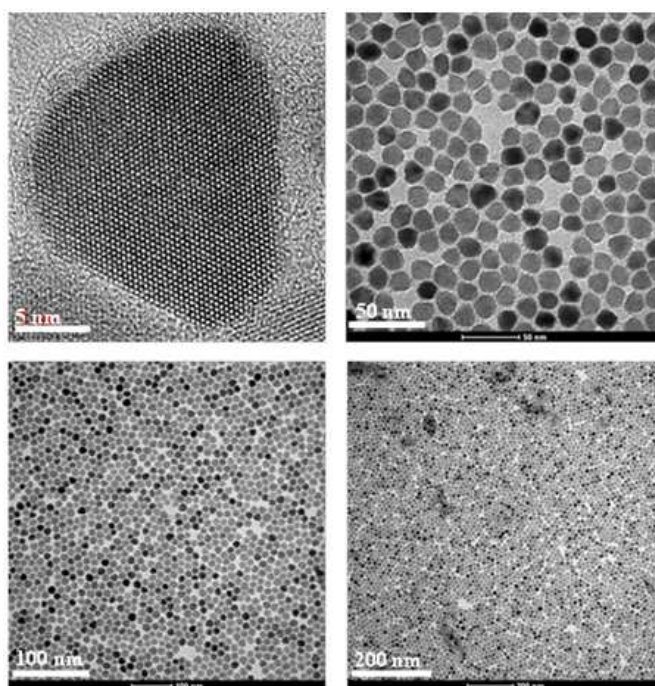


Fig. 2. TEM images of CuInSe<sub>2</sub> (CIS DPP: Se)

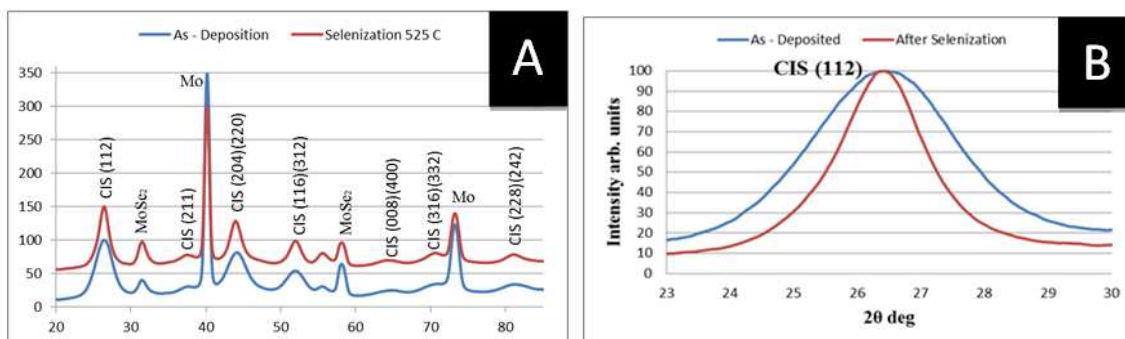


Fig. 3. XRD pattern of CIS DPP: Se: (A) as-deposited by spray-cast and after selenization, (B) comparison between CuInSe<sub>2</sub> peak (112) before and after selenization

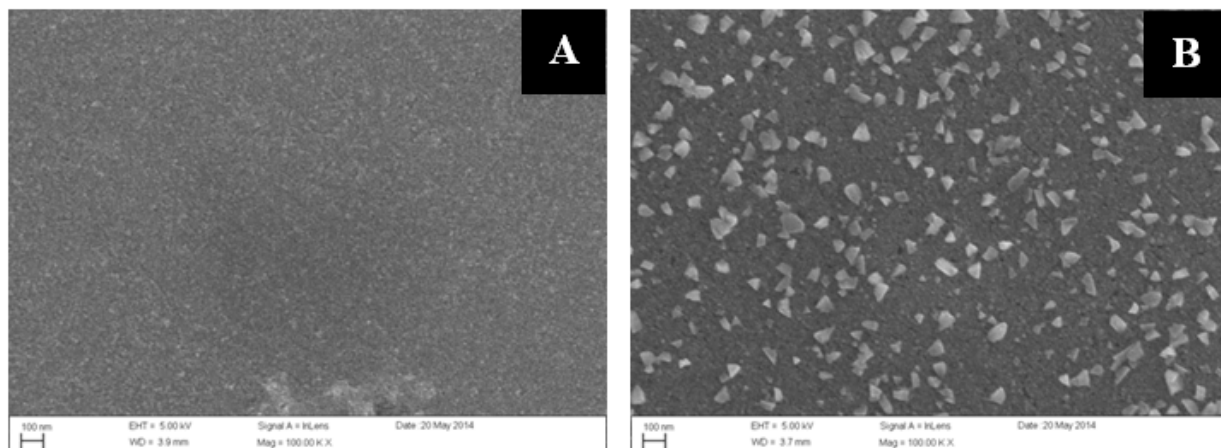


Fig. 4. SEM Images of CIS DPP: Se 150 nm layer deposited with  $10 \text{ mg mL}^{-1}$  by spray-casting: (A) before and (B) after selenization

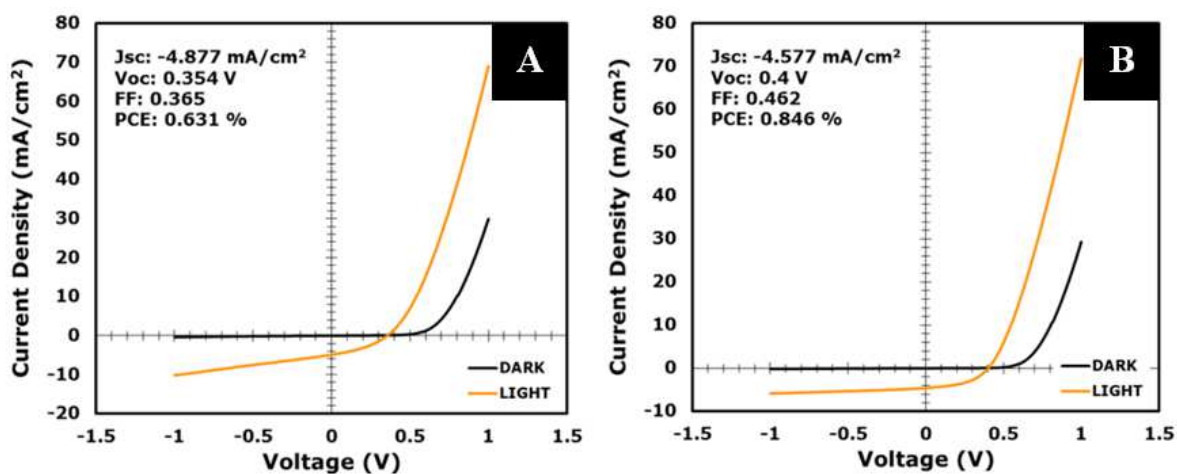


Fig. 5. I-V characteristics for Mo/CIS DPP: Se/CdS/ZnO/ITO heterojunction solar cell at thickness layer of 150 nm deposited by spray-coating: (A) as-deposited (B) after selenization

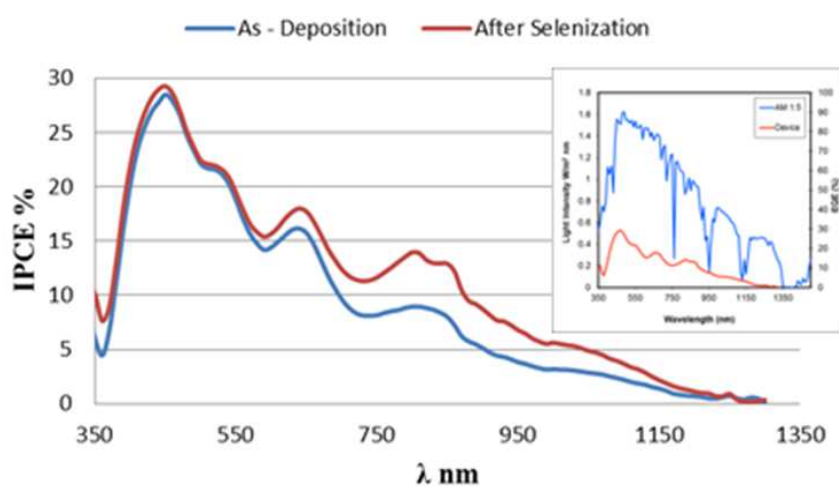


Fig. 6. IPCE measurements of Mo/CIS DPP: Se/CdS/ZnO/ITO devices

Measurements of the Incident Photon-to-electron Conversion Efficiency (IPCE) provide additional insight into how well the devices are performing and what the limiting factors are. Figure 6 The Mo/CIS DPP: Se/CdS/ZnO/ITO devices performed well under AM1.5 illumination, with a fill factor of 0.462 with a 350 nm.

The IPCE data is essentially an external quantum efficiency (at zero bias) that does not account for how much light is absorbed by the device. It is a measure of charge carriers extracted based on the number of photons that are illuminating the device. Efficient device performance of the devices is also enhanced by light reflection from the back contact. Especially, the films after selenization benefit from a "second pass" of light reflected off the back contact. This is evident in the IPCE measurements at longer wavelengths (600 nm to 1200 nm) where only a very small fraction of the incident light is absorbed by the thinner layers on the first pass. As the films get thicker, a large fraction of the incident photons are absorbed deeper in the nanocrystals layer and the resulting photogenerated carriers are unable to be efficiently extracted (Akhavan, 2011).

## Conclusion

The device architecture consisting of layers of glass/Mo/CIS/CdS/ZnO/ITO solar cell fabricated before and after selenization for thicknesses of 150 nm and concentration  $10 \text{ mg mL}^{-1}$  of CIS DPP: Senanocrystal layer deposited by spray-coating. It is clear that (PCE) increased after selenization from 0.631 to 0.846%. A prolonged selenization time could improve the intensity of diffraction peaks. The (112) peak due to the CIS become narrower after annealing at  $525^\circ\text{C}$  for 1 h in Ar atmosphere. The surface morphology shows that the CIS composition before annealing (as deposition) has a small grain size and smooth surface but become nearly uniform and dense surface with visible boundary after annealing. When annealing CIS composition, the grain size become much larger than the grain size in as-deposition composition.

## Acknowledgment

All data achieved at laboratory of chemical engineering dept.-University of Texas at Austin.

## Ethics

This article is original and contains unpublished material. The corresponding author confirms that all of the other authors have read and approved the manuscript and no ethical issues involved.

## References

- Akhavan, V.A., 2011. Photovoltaic devices based on  $\text{Cu}(\text{In}_{1-x}\text{Ga}_x)\text{Se}_2$  nanocrystal inks. PhD. Thesis, The University of Texas at Austin, Texas.
- Akhavan, V.A., B.W. Goodfellow, M.G. Panthani, C. Steinhagen and T.B. Harvey *et al.*, 2012. Colloidal CIGS and CZTS nanocrystals: A precursor route to printed photovoltaics. *J. Solid State Chem.*, 189: 2-12. DOI: 10.1016/j.jssc.2011.11.002
- Akhavan, V.A., B.W. Goodfellow, M.G. Panthani, D.K. Reid and D.J. Hellebusch *et al.*, 2010a. Spray-deposited  $\text{CuInSe}_2$  nanocrystal photovoltaics. *Energy Environ. Sci.*, 3: 1600-1600. DOI: 10.1039/C0EE00098A
- Akhavan, V.A., M.G. Panthani, B.W. Goodfellow, D.K. Reid and B.A. Korgel, 2010b. Thickness-limited performance of  $\text{CuInSe}_2$  nanocrystal photovoltaic devices. *Opt Express*, 18: A411-A420. DOI: 10.1364/OE.18.00A411
- Bindu, K., C. Sudha Kartha, K.P. Vijayakumar, T. Abe and Y. Kashiwab, 2003.  $\text{CuInSe}_2$  thin film preparation through a new selenisation process using chemical bath deposited selenium. *Solar Energy Mater. Solar Cells*, 79: 67-79. DOI: 10.1016/S0927-0248(02)00367-7
- Cullity, B.D., 1967. Elements of X-ray diffraction. Addison Wesley publishing co. Ltd London.
- Ider, M., R. Pankajavalli, W. Zhuang, J.Y. Shen and T.J. Anderson, 2014. Thermo chemistry of the  $\text{Cu}_2\text{Se-In}_2\text{Se}_3$  system. *J. Alloys Compounds*, 604: 363-372. DOI: 10.1016/j.jallcom.2014.03.129
- Katagiri, H., K. Saitoh, T. Washio, H. Shinohara and T. Kurumadani *et al.*, 2001. Development of thin film solar cell based on  $\text{Cu}_2\text{ZnSnS}_4$  thin films. *Solar Energy Mater. Solar Cells*, 65: 141-148. DOI: 10.1016/S0927-0248(00)00088-X
- McCandless, B.E. and W.N. Shafarman, 2003. Chemical surface deposition of ultra-thin semiconductors. *US Patent*, 6: 537-845.
- Parretta, A., M.L. Addonizio, A. Agati, M. Pellegrino and L. Quercia *et al.*, 1993. Influence of morphology and structure of Cu/In alloys on the properties of  $\text{CuInSe}_2$ . *Jpn. J. Applied Phys.*, 32: 80-80. DOI: 10.7567/JJAPS.32S3.80
- Schmidt, J., H.H. Roscher and R. Labusch, 1994. Preparation and properties of  $\text{CuInSe}_2$  thin films produced by selenization of co-sputtered Cu-In films. *Thin Solid Films*, 251: 116-120. DOI: 10.1016/0040-6090(94)90675-0
- Stolle, C.J., M.G. Panthani, T.B. Harvey, V.A. Akhavan and B.A. Korgel, 2012. Comparison of the photovoltaic response of oleylamine and inorganic ligand-capped  $\text{CuInSe}_2$  nanocrystals. *ACS Applied Mater Interfaces*, 4: 2757-2761. DOI: 10.1021/am3003846

- Stolle, C.J., T.B. Harvey and B.A. Korgel, 2013. Nanocrystal photovoltaics: A review of recent progress. *Curr. Opin. Chem. Eng.*, 2: 160-167. DOI: 10.1016/j.coche.2013.03.001
- Szot, J. and D. Haneman, 1984. Sol. Preparation and characterization of CuInSe<sub>2</sub> and CdS films. *Solar Energy Mater.*, 11: 289-289. DOI: 10.1016/0165-1633(84)90047-9
- Tani, Y., K. Sato and H. Katayama-Yoshida, 2012. First-principles materials design of CuInSe<sub>2</sub>-based high-efficiency photovoltaic solar cells. *Phys. B*, 407: 3056-3058. DOI: 10.1016/j.physb.2011.08.076
- Tesson, O., M. Morsli, A. Bonnet, V. Jousseume and L. Cattin *et al.*, 1998. Mase, electrical characterisation of CuInSe, thin films for solar cells applications. *Optical Mater.*, 9: 511-515. DOI: 10.1016/S0925-3467(97)00087-6
- Tzvetkova, E., N. Stratieva, M. Ganchev, I. Tomov and K. Ivanova *et al.*, 1997. Preparation and structure of annealed CuInSe<sub>2</sub> electrodeposited films. *Thin Solid Films*, 311: 101-106. DOI: 10.1016/S0040-6090(97)00263-0
- Verma, S., N. Orbey, W.B. Robert and T.W.F. Russell, 1996. Chemical reaction analysis of copper indium selenization. *Prog. Photovolt. Res. Applied*, 4: 341-353. DOI: 10.1002/(SICI)1099-159X(199609)
- Zhang, S.B., S.H. Wei, A. Zunger and H. Katayama-Yoshida, 1998. Defect physics of the CuInSe<sub>2</sub> chalcopyrite semiconductor. *Phys. Rev. B*, 57: 9642-9642. DOI: 10.1103/PhysRevB.57.9642B